Science Press

ARTICLE

Compression Bonding Behavior and Interfacial Microstructural Evolution of GH4169 Superalloy

Wang Shun,   Wang Yang,   Zhang Yuanxiang,   Fang Feng,   Ran Rong,   Yuan Guo

State Key Laboratory of Rolling and Automation (RAL), Northeastern University, Shenyang 110819, China

Abstract: In order to simulate the hot-rolling composite technology of GH4169 superalloy, the hot isothermal compression bonding tests were performed on an MSS-200 thermal simulator in the temperature range of 900 °C to 1100 °C and at strain rates of 1~10 s^{-1}. The Arrhenius type constitutive equation and the hot processing map were established to describe the deformation behavior of GH4169 superalloy during the compression bonding. Furthermore, the corresponding thermal deformation activation energy Q and the stress index n were calculated as 320.33 kJ·mol^{-1} and 4.1573, respectively. Additionally, the bonding interfaces were observed by optical microscope (OM) and electron backscatter diffraction (EBSD) technique. The results show that the bonding interface is mainly affected by the technological parameters, and the bonding interface becomes almost invisible at 1100 °C with a rate of 10 s^{-1}.

Key words: GH4169 superalloy; hot compression bonding; deformation behavior; interfacial microstructure

GH4169 nickel-based superalloy has excellent corrosion resistance and good weldability, as well as high strength at elevated temperature up to 650 °C[1-3]. Therefore, it is widely used in the manufacture of aircraft engines, marine gas turbines and the key components of land-based gas turbines[4-6]. It is well known that the hot deformation parameters play a crucial role in determining the microstructure evolution and mechanical properties of this material. During the past several decades, the hot deformation behavior of GH4169 superalloy has been widely studied using hot tensile or hot compression experiments[7-11]. Many scholars have proposed some dynamic models to describe the relationship between flow stress and process parameters, and the microstructure evolution of GH4169 superalloy in different processes was investigated in-depth[12-15].

In recent years, in order to improve the elemental segregation behavior of large size ingot, a metal construction forming technology has been proposed[16,17]. The homogeneous small size billets were firstly obtained, and then subjected to surface treatment, stacking and vacuum package, and after that, the large deformation at high temperature was applied to realize the composite forming. Using this novel technology,

the microstructure homogeneity of large products of GH4169 superalloy can be well improved. So it has very important engineering significance for the research on hot compression bonding behavior of GH4169.

In the previous thermal simulation tests on GH4169 superalloy, most of the studies were conducted on a single sample, and the research on its thermal deformation behavior has been well developed. In recent years, some researchers have started preliminary study on the hot compression bonding behavior. Yang et al[18] simulated the flow behavior of GH4169 superalloy during linear friction welding, and characterized the deformation behavior of GH4169 superalloy during compression by establishing a constitutive Arrhenius type equation. Geng et al[14] studied the thermal deformation behavior and finite element simulation during linear friction welding of GH4169 superalloy. According to the measured flow stress-strain data, three constitutive equations based on the modified strain compensated Arrhenius model, Johnson-Cook (J-C) model and Field-Backofen (F-B) model were derived. They found that the strain compensated Arrhenius model is more suitable for LFW numerical simulation of GH4169 superalloy. Yang et al[19] simulated the interfacial

microstructure evolution of GH4169 of LFW joints during hot compression bonding, the interfacial defects were observed by scanning electron microscope (SEM), and the interfacial oxidation of the welded joints was discussed. Zhang et al[5,20,21] systematically investigated the plastic deformation bonding behavior of IN718 superalloy, and reported that the bonding strength of the interface is significantly enhanced with the increase of deformation temperature and strain. Meanwhile, EBSD and TEM results revealed that the bonding of joints is related to the interfacial grain boundary bulging.

However, in actual rolling production, according to the accurate calculation method of rolling strain rate parameter $\dot{\varepsilon}$ proposed by Zhao[22], the required strain rate for hot rolling is in the range of 1~10 s^{-1}. But in the previous literatures, few detailed and in-depth studies were reported in the range of 1~10 s^{-1}. Therefore, a more accurate model is needed for GH4169 in practical engineering applications. In this work, the hot compression bonding tests were performed on an MSS-200 thermal simulator at 900~1100 °C and 1, 3, 5, 7, 10 s^{-1}, and the constitutive equation of GH4169 superalloy was established during compression bonding. Additionally, the evolution of interface microstructure of GH4169 was also observed. The tests carried out in this study at a high strain rate can better simulate the rolling composite process of GH4169, so it can provide theoretical guidance for the actual rolling composite technology of GH4169.

1 Experiment

The chemical composition (wt%) of GH4169 superalloy is given as follows: Ni 52.62, Cr 18.23, Nb 5.11, Mo 2.98, Ti 0.98, Al 0.50, Co 0.16, C 0.03 and Fe balance. Fig.1 shows the detailed experimental process of hot compression bonding. The sample is a cylinder with a diameter of 8 mm and a height of 12 mm. As show in Fig.1, a set of two samples were simultaneously heated to different deformation temperatures at a heating rate of 5 °C/s, then held for 300 s to homogenize their microstructures, and finally compressed for bonding. Hot compression bonding tests were conducted on an MMS-200 thermal simulator at the strain rate of 1, 3, 5, 7, and 10 s^{-1} in the temperature range of 900~1100 °C, and the engineering compressive strain of all samples was 60%. The flow stress-
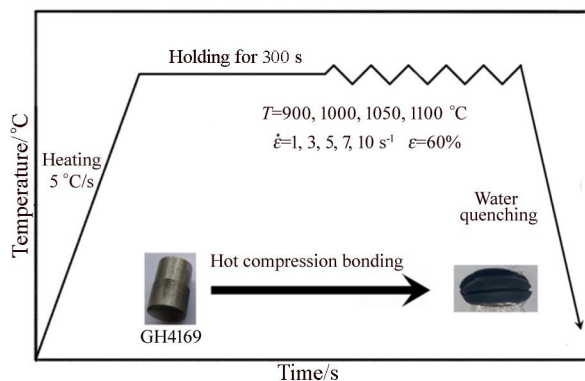
strain curves were firstly analyzed, and then the Arrhenius-type constitutive equation and hot working map were established to describe the compression bonding deformation behavior of GH4169 superalloy. In order to observe the microstructure evolution of the bonding interface, the bonded samples were cut along the direction of compression, and the OM and EBSD techniques were applied. The OM samples were prepared by standard mechanical polishing procedures and etched in a hydrochloric acid solution (5 g H_2O_2+100 mL HCl+100 mL C_2H_5OH). The EBSD samples were electropolished in a solution of ethanol and perchloric acid (20:1). The electrolysis voltage was 25 V and the current was 1 A.

2 Results and Discussion

2.1 Flow curves

The flow behaviors of GH4169 superalloy under various test conditions are presented in Fig.2 and Fig.3. It is well accepted that the flow stress of hot compression samples is mainly reflected in the competition between work hardening and dynamic softening. It can be found that the flow stress increases rapidly as the true strain increases at the initial deformation stage, which is attributed to the work hardening caused by the dislocation multiplication. Meanwhile, the dynamic recovery during this stage is too weak to balance the effects of work hardening. Subsequently as the deformation proceeds, the dynamic recrystallization will occur when the accumulated dislocation density exceeds a critical strain, which decreases the work hardening rate. After reaching the peak stress, it is decreased slightly to a steady-state value due to the evident dynamic softening induced by dynamic recrystallization[14,18,23]. It can be seen from Fig.2 that the flow stress decreases with the increase of deformation temperature at the same strain rate, and the degree of flow stress reduction increases with the reduction of deformation temperature. Higher temperatures are followed by stronger thermal activation processes. With the increase of temperature, the nucleation rate and growth rate of dynamic recrystallization increase and the softening effect of recrystallization is strengthened. At this time，the dislocation also has enough activity to overcome the pinning effect of the metal deformation structure on it and make a certain movement, which is manifested by cross slip of screw dislocation and climb motion of edge dislocation.

As shown in Fig.3, during the isothermal deformation, the flow stress increases with increasing strain rate, and the extent of the decline of flow stress increases with the increase of the strain rate. Overall, the peak stress is the smallest at the low strain rate of 1 s^{-1}, and with the increase of strain rate from 1 s^{-1} to 10 s^{-1} at 1000 °C, the peak stress increases from 330 MPa to 540 MPa. Therefore, when the temperature is constant, the level of dynamic recrystallization is increased as the strain rate decreases. The GH4169 superalloy shows evident peak stress at a high strain rate of 5~10 s^{-1}, followed by a sharp decrease in flow stress, indicating that the softening

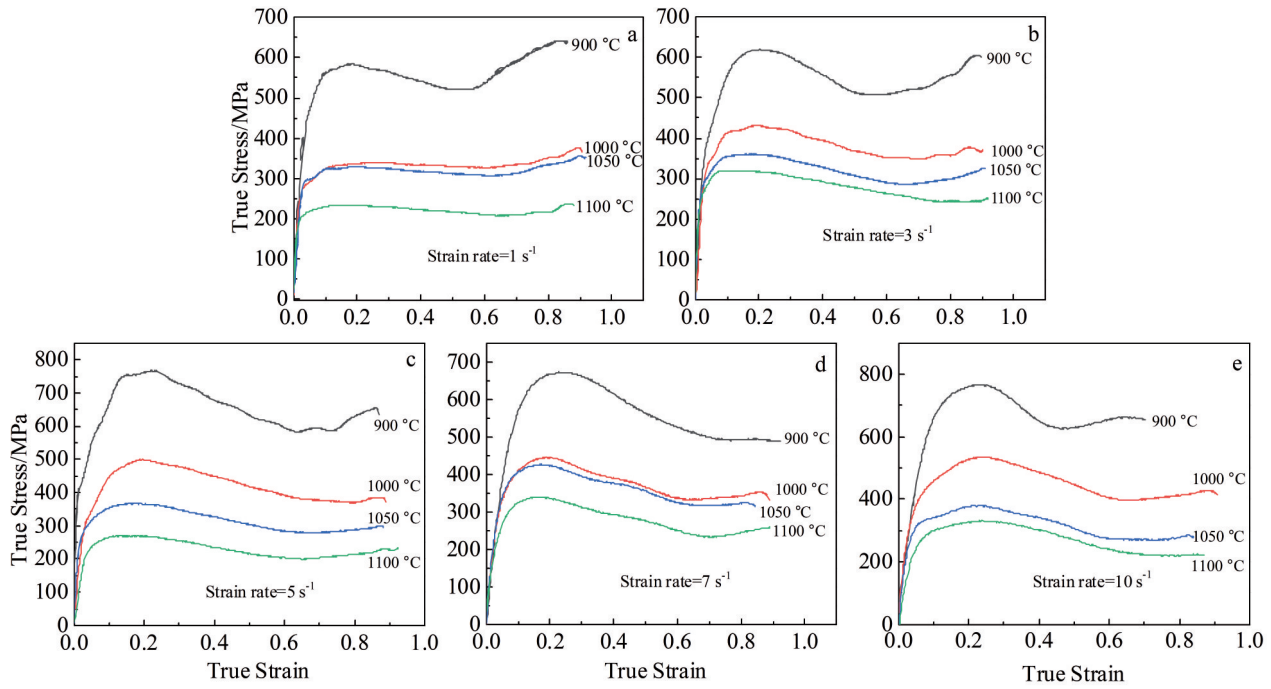Fig.1　Experimental process of GH4169 superalloy

Fig.2   True stress-true strain curves of GH4169 superalloy during hot compression bonding at different strain rates: (a) 1 s⁻¹, (b) 3 s⁻¹, (c) 5 s⁻¹, (d) 7 s⁻¹, and (e) 10 s⁻¹
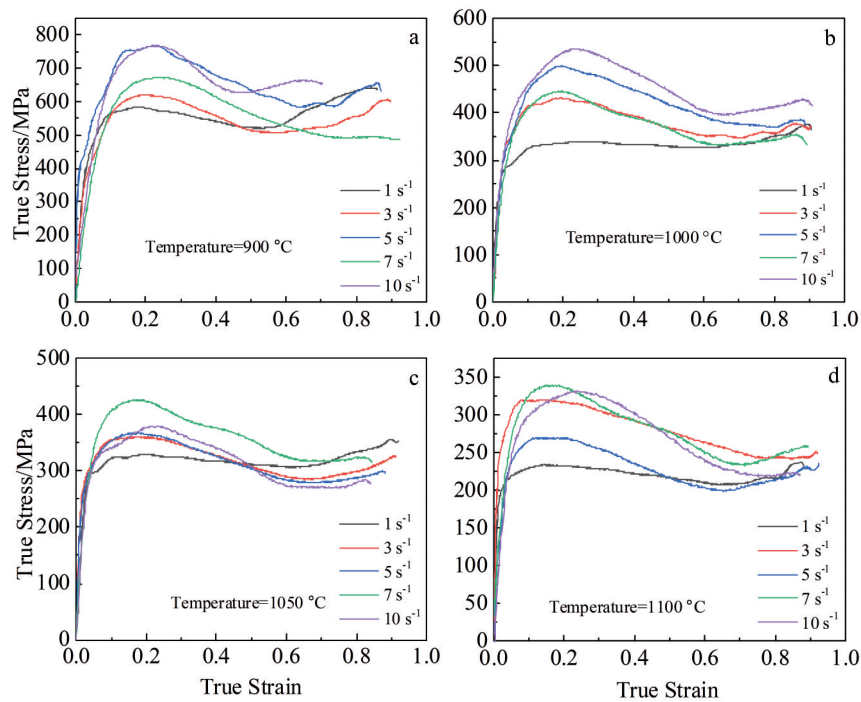

Fig.3   True stress-true strain curves of GH4169 superalloy during hot compression bonding at different deformation temperatures: (a) 900 °C, (b) 1100 °C, (c) 1050 °C, and (d) 1100 °C

mechanism is dominant with the progress of deformation. The stress slightly increases at the last stage of deformation, and the reason is that the friction between the sample and the die increases with the increase of deformation, which is ultimately reflected in the increase of flow stress.

2.2 Constitutive equation

The mathematical expression derived from the functional relationship between stress and strain rates of materials is usually called constitutive equations, which is used to describe the rheological properties of materials and is the basis for optimizing the deformation process. In order to describe the hot deformation behavior of GH4169 superalloy and predict high-temperature flow stress during the compression bonding, the Arrhenius constitutive model was established. The flow

stress can be modeled not only to obtain model equations for the hot deformation of the alloy, but also to calculate the activation energy and identify deformation parameters leading to various deformation mechanisms.

The relationship between the flow stress, the strain rate and the deformation temperature during hot deformation can be expressed by several basic equations as follows:

$$\dot{\varepsilon} = A_1 \sigma^{n_1} \exp(-Q/RT) \quad \alpha\sigma < 0.8 \quad (1)$$

$$\dot{\varepsilon} = A_2 \exp(\beta\alpha) \exp(-Q/RT) \quad \alpha\sigma < 1.2 \quad (2)$$

$$\dot{\varepsilon} = A[\sinh(\alpha\sigma)]^n \exp(-Q/RT) \quad \text{all } \sigma \quad (3)$$

$$Z = \dot{\varepsilon} \exp(-Q/RT) = A[\sinh(\alpha\sigma)]^n \quad (4)$$

where $\dot{\varepsilon}$ is the strain rate (s^{-1}), σ is the peak stress (MPa), Q is the hot deformation activation energy (J·K^{-1}·mol^{-1}), R is the gas constant (8.3145 J·K^{-1}·mol^{-1}), T is the deformation temperature (K), A_1, A_2, A, n_1, β and n are material constants, α is an adjustable constant (MPa^{-1}), and Z is a Hollomon parameter (s^{-1}).

Eq.(5) and Eq.(6) can be got by taking the logarithm on both sides of Eq.(1) and Eq.(2)

$$\ln\dot{\varepsilon} = n_1 \ln\sigma + \ln A_1 - Q/RT \quad (5)$$

$$\ln\dot{\varepsilon} = \beta\sigma + \ln A_2 - Q/RT \quad (6)$$

Substituting the peak stress σ under different thermal deformation conditions into Eq.(5) and Eq.(6), the linear fitting curve of $\ln\dot{\varepsilon}$ - $\ln\sigma$ and $\ln\dot{\varepsilon}$ - σ can be obtained under different deformation conditions, as shown in Fig.4. Then the average value of the straight lines was calculated, and the value of n_1 and β are 5.7622 and 0.0138 MPa^{-1}, respectively. Finally, through the relation $\alpha=\beta/n_1$, we get α =0.002 398 8.
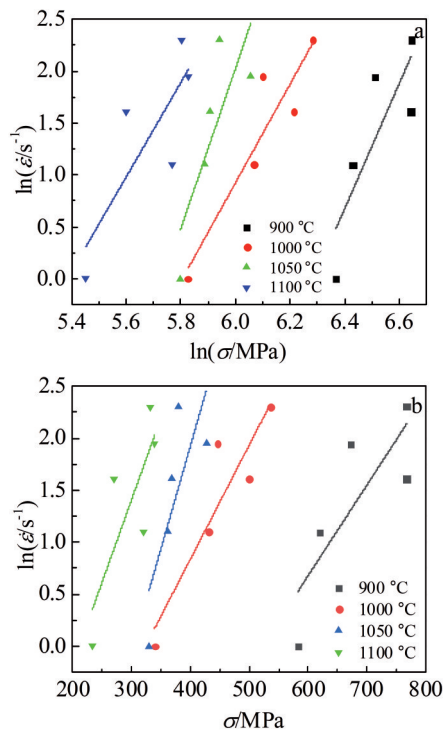
Taking the logarithm for Eq.(3), it can be expressed as:

Fig.4　Relationship of $\ln\dot{\varepsilon}$-$\ln\sigma$ (a) and $\ln\dot{\varepsilon}$-σ (b)

$$\ln\dot{\varepsilon} = n[\sinh(\alpha\sigma)] + \ln A - Q/RT \quad (7)$$

Supposing that the deformation activation energy is independent of temperature, for a particular strain rate condition, the logarithm of Eq.(3) can be expressed as:

$$\ln[\sinh(\alpha\sigma)] = \frac{\ln A - \ln\dot{\varepsilon}}{n} + \frac{Q}{nR}\frac{1}{T} \quad (8)$$

Fig.5a shows the relationship between $\ln\dot{\varepsilon}$ and $\ln[\sinh(\alpha\sigma)]$. Fig.5b shows the relationship between $\ln[\sinh(\alpha\sigma)]$ and $1/T$. Through linear regression, the average values of n and Q are 4.1573 and 320.327 J·K^{-1}·mol^{-1}, respectively.

Eq.(3) can also be expressed as

$$\ln Z = \ln A + n\ln[\sinh(\alpha\sigma)] \quad (9)$$

The relationship between $\ln Z$ and $\ln[\sinh(\alpha\sigma)]$ is shown in Fig.5c, and the value of correlation coefficient R is 0.944 91, revealing a good linear relation.

Therefore, the constitutive equation of GH4169 superalloy during the hot compression bonding at a strain of 0.92 can be written as:

$$\dot{\varepsilon} = 3.42498 \times 10^{13}[\sinh(0.002399\sigma)]^{4.157333}$$
$$\times\exp(-320327/RT) \quad (10)$$

2.3 Processing map

Processing maps can effectively predict the quality of the hot working performance of the metal material, and its establishment is an important link to determine the material process parameters, which can help to avoid unstable areas and find areas with high consumption values. The objective of the present work is to investigate the deformation behaviors of GH4169 superalloy by establishing the hot processing maps for optimizing the forging processes.

After further modifying the original model, Prasad proposed a dynamic material model (DMM). In this article, the DMM was applied to draw the thermal processing diagram of GH4169 superalloy. During the thermal processing of the material, the total energy P (J) absorbed by the unit volume of the material from the outside world is converted into the grain boundary misorientation distribution plots and the power co-content:

$$P = \sigma\dot{\varepsilon} = G + J = \int_0^{\dot{\varepsilon}} \sigma\mathrm{d}\dot{\varepsilon} + \int_0^{\sigma} \dot{\varepsilon}\mathrm{d}\sigma \quad (11)$$

The sensitivity factor m indicates how much energy is consumed:

$$m = \left(\frac{\mathrm{d}J}{\mathrm{d}G}\right)_{\varepsilon,T} = \left(\frac{\partial\ln\sigma}{\partial\ln\dot{\varepsilon}}\right) \quad (12)$$

The dissipation factor η represents the ratio of the dissipation covariance in the thermoplastic process to the linear dissipation covariance:

$$\eta = \frac{J}{J_{\max}} = \frac{2m}{m+1} \quad (13)$$

According to the irreversibility principle of thermodynamics, the rheological instability is determined by:

$$\zeta(\varepsilon) = \frac{\partial\ln\left(\dfrac{m}{m+1}\right)}{\partial\ln\varepsilon} + m < 0 \quad (14)$$

The power dissipation factor and the instability factor are obtained by fitting the η of each strain rate at different temperatures with the cubic B-spline interpolation, and the
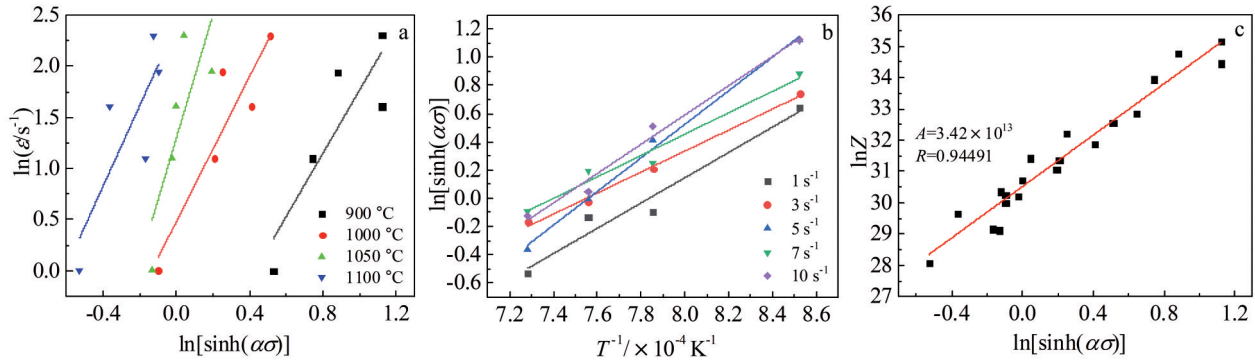
Fig.5　Linear relationship of $\ln\dot{\varepsilon}$-$\ln[\sinh(\alpha\sigma)]$ (a), $\ln[\sinh(\alpha\sigma)]$-$1/T$ (b), and $\ln Z$-$\ln[\sinh(\alpha\sigma)]$ (c)

thermal processing map of GH4169 superalloy is formed by coupling and superposition (Fig.6).

Fig. 6 is a processing map of GH4169 superalloy at temperatures of 900~1100 °C and strain rates of 1~10 s^{-1}. The maps are classified into two domains: the contour numbers represent power dissipation efficiency and the shaded domains indicate the regions of flow instability. As can be seen from Fig.6 that the high dissipation values on the contours are concentrated in the upper right areas. Domain with such a peak efficiency values of power dissipation is typical of the dynamic recrystallization (DRX) process for nickel materials. The stability domain extends over a temperature range of 1070 °C to 1100 °C at strain rates exceeding 7.3 s^{-1}. According to this, GH4169 superalloy has the best process performance at the temperature of 1070~1100 °C and strain rate of 7.3~10 s^{-1}.

Meanwhile, the material exhibits two instability domains at relatively low strain rates: one appears in a range of 900~950 °C with the strain rate of 1~1.6 s^{-1} and the other is 950~1100 °C with a strain rate of 1~4.48 s^{-1}. As the temperature increases, the instability domain moves toward intermediate. And the twins, adiabatic shear bands, and cavities will appear in this domain. Therefore, GH4169 superalloy should avoid this technological parameter during the hot working process.

3　Microstructure

3.1　Microstructural characteristics of the bonding area

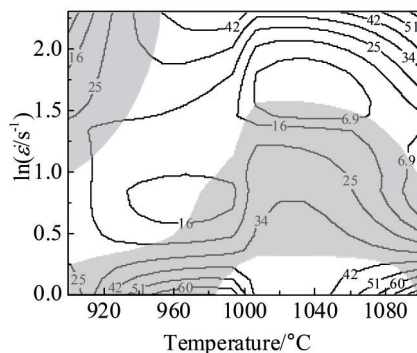Fig. 7 shows metallographic images of the microstructure

Fig.6　Processing map of GH4169 superalloy at a strain of 0.92

evolution at the bonding interfaces at the temperatures (T) of 900~1100 °C and strain rates ($\dot{\varepsilon}$) of 1~10 s^{-1}. During the hot compression bonding process of GH4169, temperature, strain rate, surface roughness and deformation amount all have a significant impact on the bonding interface. It can be observed that the bonding interface in the center of sample is almost completely straight at high temperatures and high strain rates. It is worth mentioning that the bonding interface becomes almost invisible when the temperature is 1100 °C at the strain rate of 5~10 s^{-1}. In particular, the bonding interface is irregular at low strain rates of 1~3 s^{-1} while it becomes flat and neat with the increase of temperature and strain rate, indicating that the GH4169 superalloy has a significant bonding effect under this technological parameter.

3.2　Dynamic recrystallization in the bonding area

The above analysis of the stress-strain curves shows that different levels of dynamic recrystallization occur during the deformation process. To further explore the evolution of microstructure, recrystallized behavior was analyzed in detail by EBSD. The typical inverse pole figures (IPF) in Fig.8a~8d show the effects of temperature on the interfacial microstructure evolution of GH4169 superalloy. It can be seen that the structure in the bonding interface is characterized by a chain of fine pancake-shaped grains at 900 °C, and with the increase of temperature, the fine pancake-shaped grains fades away. Meanwhile, the new grains appearing along the boundary of the original grain grow up continuously until the interface gradually disappears. It is worth noting that the average grain size increases from 2 μm at 900 °C to 19 μm at 1100 °C while it is 5 μm at 1000 °C and 11 μm at 1050 °C. Significantly, the grain size is mainly affected by temperature and the grain growth at the bonding interface is the reason for the disappearance of the interface. As shown in Fig.8e~8i, the average proportion of recrystallization and substructure are 49% and 47% while the proportion of deformation in the bonding interface region is low. The recrystallized grains growing along the bonding interface pass through the interface and promote the interfacial bonding.

As we know, the interfacial microstructure is closely related to the processing temperature and strain rate. The microstructure evolution at the same strain rate has been analyzed above, and Fig.9 shows the evolution of the bonding
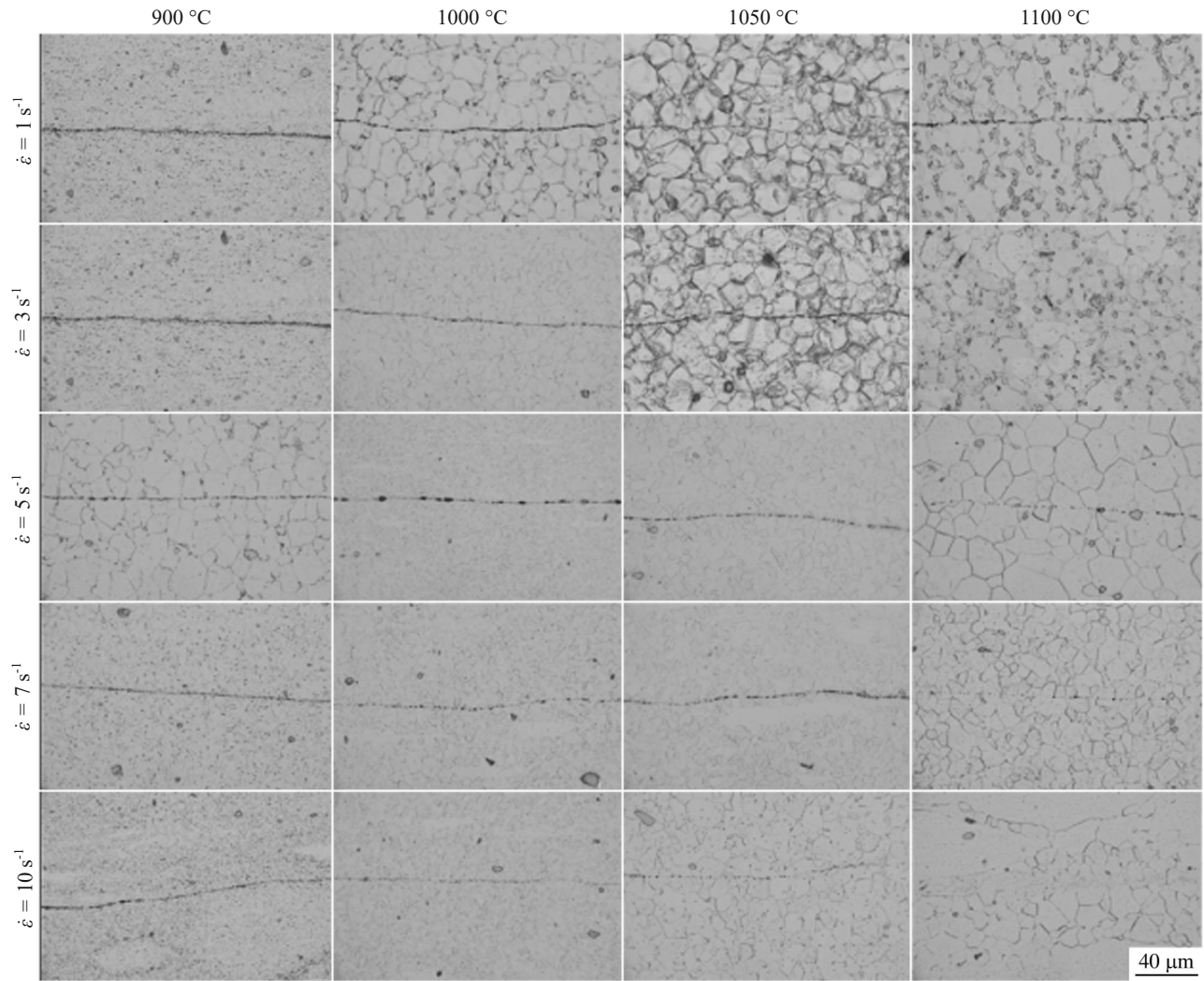
Fig.7   OM images of the bonding area of obtained joints under different bonding temperatures and strain rates
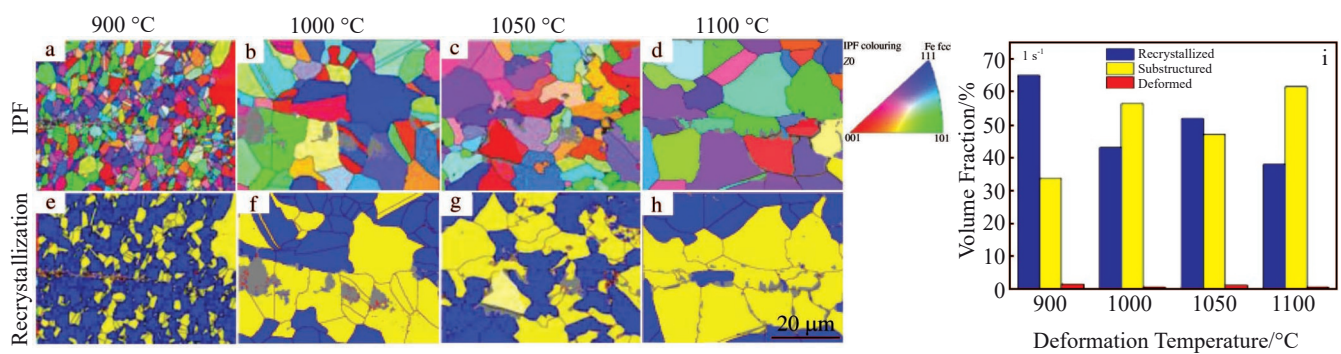

Fig.8   Microstructural evolution of GH4169 superalloys at the strain rate of 1 s⁻¹ and various deformation temperatures

interfacial microstructures which involve both high and low strain rates and temperatures. As shown in Fig. 9a and 9b, a large number of small equiaxed grains appear after deformation. At 900 °C, the average grain size is 2 μm at 1 s⁻¹ and 1.8 μm at 10 s⁻¹ while it is 19 μm at 1 s⁻¹ (1100 °C) and 21 μm at 10 s⁻¹ (1100 °C). The peak precipitation temperature of δ strengthening phase is about 900 °C, so that the high strength

δ phase results in very small grain sizes at this time. It can also be seen from the stress-strain curve in Fig. 2a that the peak stress reaches 600 MPa at 900 °C, while the peak stress is below 250 MPa at 1100 °C. Therefore, significant grain growth occurs after complete recrystallization at 1100 °C. In particular, almost all grains in the bonding interface are occupied by subgrains at 1100 °C with a strain rate of 10 s⁻¹,

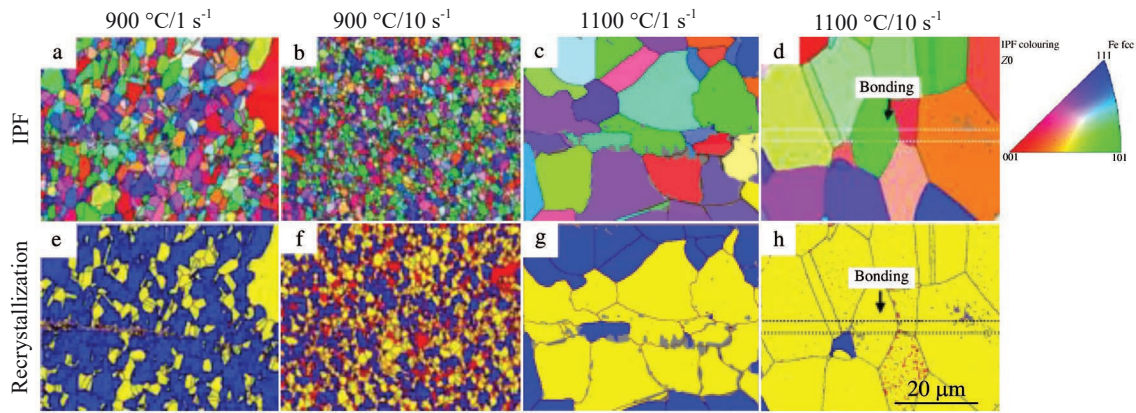900 °C/1 s⁻¹ 900 °C/10 s⁻¹ 1100 °C/1 s⁻¹ 1100 °C/10 s⁻¹

Fig.9 Microstructural evolution of GH4169 at the deformation temperature of 900 °C and 1100 °C with strain rates of 1 s⁻¹ and 10 s⁻¹

and the bonding interface is almost invisible at this time. The IPF diagrams in Fig.8 and Fig.9 show that the grain size in the bonding interface is the largest, and gradually decreases along the two ends of the interface. The reason may be that the stress cannot be transferred to the interface in time during compression deformation, and the recrystallization and grain growth occurs in the bonding interface before crushing.

4 Conclusions

1) The calculated values of constitutive model parameters Q and n of GH4169 superalloy are 320.33 J·K⁻¹·mol⁻¹ and 4.1573, respectively. On this basis, the Arrhenius type thermal deformation constitutive equation can be established.

2) The processing map shows the best process performance of GH4169 superalloy when the temperature is 1070~1100 °C and the strain rate is 7.3~10 s⁻¹.

3) Combined with the processing map and the microstructure observation, the optimal deformation parameters for interface bonding are 1100 °C and 5~10 s⁻¹.

References

1 Li Guangyao, Zhang Zheshuo, Sun Guangyong *et al. International Journal of Mechanical Sciences*[J], 2014, 89: 439 (in Chinese)

2 Pradhan D, Mahobia G, Chattopadhyay K *et al. International Journal of Fatigue*[J], 2018, 114: 120

3 Xu Jinghao, Huang Zaiwang. *Materials Science & Engineering A* [J], 2017, 690(6): 137

4 Yuan Kangbo, Guo Weiguo, Li Penghui *et al. Materials Science & Engineering A*[J], 2018, 721: 215

5 Zhang Jianyang, Xu Bin, Naeemul H T *et al. Journal of Materials Science & Technology*[J], 2020, 46: 1 (in Chinese)

6 Sun Guoqin, Wang Dong, Shang Degang. *Fatigue & Fracture of Engineering Materials & Structures*[J], 2013, 36: 1039 (in Chinese)

7 Al Saadi M, Mu Wangzhong, Hulme S N. *Metals-Open Access*

Metallurgy Journal[J], 2020, 11(1): 36

8 Wang Yujing, Shao Wenzhou, Li Yang *et al. Materials Science & Engineering A*[J], 2008, 497(1-2): 479

9 Wang Zhongtang, Zhang Shihong, Cheng Ming *et al. Journal of Iron and Steel Research International*[J], 2010, 17(7): 75 (in Chinese)

10 Yuan Hui, Liu Wangchang. *Materials Science & Engineering A* [J], 2005, 408(1-2): 281

11 Cabrera J M, Ponce J, Prado J M. *Journal of Materials Processing Technology* [J], 2003, 143: 403

12 Geng Peihao, Qin Guoliang, Zhou Jun *et al. Journal of Materials Processing Technology*[J], 2020, 288 (in Chinese)

13 Chen Rongchuang, Zhang Zhizhen, Li Jianjun *et al. Crystals*[J], 2018, 8(7): 282 (in Chinese)

14 Geng Peihao, Qin Guoliang, Zhou Jun *et al. Journal of Manufacturing Processes*[J], 2018, 32: 469 (in Chinese)

15 Lin Yongcheng, Chen Dongdong, Nong Fuqi *et al. Vacuum*[J], 2017, 137: 104 (in Chinese)

16 Sun Mingyue, Xu Bin, Li Dianzhong *et al. Chin Sci Bull*[J], 2020, 27 (in Chinese)

17 Sun Mingyue, Xu Bin, Xie Bijun *et al. Journal of Materials Science & Technology*[J], 2021, 71: 84 (in Chinese)

18 Yang Xiawei, Li Wenya, Ma Juan *et al. Journal of Alloys and Compounds*[J], 2016, 656: 395

19 Yang Xiawei, Li Wenya, Feng Yan *et al. Materials & Design*[J], 2016, 104(15): 436 (in Chinese)

20 Zhang Jianyang, Sun Mingyue, Xu Bin *et al. Metallurgical and Materials Transactions B*[J], 2018, 49: 2152

21 Zhang Jianyang, Xu Bin, Naeemul H T *et al. Journal of Materials Science and Technology*[J], 2020, 40: 54 (in Chinese)

22 Zhao Dewen, Tie Weiqi. *J Appl Sci*[J], 1995(1): 103

23 Lin Yongcheng, Chen Xiaoming, Wen Dongxu *et al. Computational Materials Science*[J], 2014, 83(2): 282 (in Chinese)

GH4169高温合金的压缩结合行为及界面组织演变

王　顺，王　洋，张元祥，方　烽，冉　蓉，袁　国

(东北大学 轧制技术及连轧自动化国家重点实验室，辽宁 沈阳 110819)

摘　要： 为了模拟GH4169高温合金的热轧复合工艺，采用MSS-200热模拟机对GH4169高温合金进行热压缩复合模拟，变形温度为900~1100 ℃，应变速率为1~10 s⁻¹。通过应力应变曲线建立了描述GH4169高温合金压缩变形行为的Arrhenius型本构方程和热加工图，计算相应的热变形活化能Q和应力指数n分别为320.33 kJ·mol⁻¹和4.1573。此外，采用光学显微镜（OM）和电子背散射衍射（EBSD）技术观察了结合界面。结果表明：结合界面主要受变形工艺参数的影响，在1100 ℃/10 s⁻¹变形条件下，结合界面几乎看不见。

关键词： GH4169高温合金；热压缩复合；变形行为；界面微观结构